Thickness dependence of magnetic properties of Ir/FeV-based systems

Djoudi Ourdani,[1] Yves Roussigné,[1] Salim Mourad Chérif,[1] Mihai Sebastian Gabor,[2,*] and Mohamed Belmeguenai[1,†]

[1]*Université Sorbonne Paris Nord, LSPM, CNRS, UPR 3407, F-93430 Villetaneuse, France*

[2]*Center for Superconductivity, Spintronics and Surface Science, Physics and Chemistry Departament, Technical University of Cluj-Napoca, Str. Memorandumului No. 28 RO-400114 Cluj-Napoca, Romania*

(Received 24 November 2022; revised 6 February 2023; accepted 10 February 2023; published 20 March 2023)

Ir-buffered $Fe_{0.7}V_{0.3}$ (FeV) thin films of variable thickness (1.4 nm $\leqslant t_{FeV} \leqslant$ 10 nm) were sputtered on thermally oxidized Si substrate and capped with Cu or MgO films. Vibrating sample magnetometery measurements allowed deducing their magnetization at saturation and the magnetic dead layer thickness, found to be capping layer independent. Microstrip line ferromagnetic resonance measurements under in-plane and perpendicular to the film plane applied magnetic fields are employed to investigate the perpendicular magnetic anisotropy (PMA) and damping. PMA is found to result from a uniaxial interfacial contribution which is slightly capping layer dependent. In contrast, the second-order PMA constant, which could result from the inhomogeneous distribution and the spatial fluctuations at the nanoscale of the uniaxial PMA at interface, is significantly stronger for Ir/FeV/Cu films. The damping dependence on the inverse of FeV effective thickness revealed a low Gilbert damping constant for FeV ($\alpha_{FeV} = 1.7 \times 10^{-3}$) and allowed concluding that damping enhancement is mainly induced by Ir/FeV. The zero frequency linewidth for in-plane configuration is attributed to two magnon scattering contribution, found to be higher for Cu capped FeV. The investigation of the FeV thickness dependence of interfacial Dzyaloshinskii-Moriya interaction (iDMI) of both systems via Brillouin light scattering allowed to conclude to the zero iDMI constant of FeV/Cu. It also led to deduce iDMI constants of Ir/FeV and FeV/MgO, estimated to be $D_s^{Ir/FeV} = (0.13 \pm 0.02)$ pJ/m et $D_s^{FeV/MgO} = (-0.07 \pm 0.02)$ pJ/m, respectively.

DOI: 10.1103/PhysRevMaterials.7.034408

I. INTRODUCTION

In order to achieve faster, denser and more efficient spintronic devices with a reduced power consumption, the magnetic material parameters have to be well defined and tuned according to the desired application. Magnetic damping, which is one of these most critical material parameters, plays important roles in many spintronic applications, since it strongly affects the energy required and the speed at which a spintronic device can operate. The most common measure of damping is the parameter α, which is usually referred to as the Gilbert damping constant. Therefore, magnetic materials having both low damping and low magnetization at saturation (M_s) are highly desirable for energy-efficient operation. Indeed, the critical current density for a spin-transfer-torque magnetic random-access memory cell is proportional to both M_s and α, the speed of domain-wall motion in racetrack memory is generally inversely proportional to α and the threshold current for auto-oscillations in spin-torque nano-oscillator scales with α [1]. Moreover, damping determines the efficiency of magnonics devices since it is correlated to the spin wave diffusions length [2]. The moderate M_s yields a reduced stray field, allowing for denser patterned structures because coupling between bits is low. Furthermore, the low damping constant, the low M_s as well as the low effective anisotropy allow for efficient reversal of magnetization through damping-like spin-orbit torque (SOT) due to the spin-Hall effect (SHE) [3].

Intrinsic damping is largely driven by the details of the band structure [4–6], especially the density of states at the Fermi level, thus the presence of conduction electrons, which lead to significant magnon-electron scattering contributions [7], limits achieving ultralow damping. Therefore, ultralow damping can be attained in insulating ferrimagnets due to the suppression of magnon-electron scattering. However, insulators cannot be used in most spintronic applications, where a charge current through the magnetic material is required. Heusler alloys are another promising group of materials for which low damping was measured [8,9]. Moreover, besides their theoretically predicted half-metallic character (perfectly spin-polarized conduction electrons at Fermi energy) at room temperature, they have the advantage of a good lattice matching with major substrates and high Curie temperature resulting in very high performances of spintronic devices. However, their magnetic and electronic properties are strongly influenced by the atomic arrangement (chemical disorder), which is primarily responsible for decreased spin polarization. Furthermore, important research effort is being put into their fabrication, since their deposition processes require relatively high temperature annealing and substrate preparation. Another alternative to achieve lower damping values is the use of iron-vanadium alloys (FeV). Indeed, It was reported that FeV is one of the best candidates for an effective reduction of the magnetization, together with a decrease of the damping [10].

*mihai.gabor@phys.utcluj.ro

†belmeguenai.mohamed@univ-paris13.fr

 ©2023 American Physical Society

To achieve nanoscale spin-transfer-torque devices with better performance, one requires larger perpendicular magnetic anisotropy for higher thermal stability. Furthermore, systems consisting of ferromagnetic and heavy metals are of extreme importance in the field of spintronics. The spin currents through the interface of such a heterostructure are at the origin of many phenomena such as spin pumping and SHE [11], which can be used for magnetization switching via SOT. This latter one is a potentially energetically efficient way to control the magnetization dynamics and, thus, emerges as an efficient mean to switch magnetization and drive novel chiral magnetic textures, such as skyrmions and domain walls [12]. Interfacial Dzyaloshinskii-Moriya interaction (iDMI) [13], which appears in heavy metal/ferromagnetic film (FM)-based systems, is of great importance for the next-generation spintronic memory devices. Therefore, the aim of this paper concerns the investigation of the damping, perpendicular magnetic anisotropy (PMA) and iDMI in Ir/FeV-based systems. The idea is to control their strength via optimizing the interface quality through the variation of FeV thickness and the use of different capping layers (Cu and MgO). For this purpose, ferromagnetic resonance (FMR), Brillouin light scattering (BLS) coupled to vibrating sample magnetometery (VSM) techniques were used.

II. SAMPLES AND EXPERIMENTAL TECHNIQUES

The studied samples are 5×5 nm^2 in size and have the structure Si/SiO_2/Ta (2.5)/Ir (4)/FeV (t_{FeV})/Cu (2) or MgO (1)/Ta (2.5), where the numbers in parentheses represent the thickness in nm and were grown using a magnetron sputtering system with a base pressure lower that 2×10^{-8} Torr. The metallic layers were deposited using dc sputtering under an Ar pressure of 1.5 mTorr, while the MgO layer was grown by rf sputtering in an Ar pressure of 10 mTorr. The FeV films were deposited from a $Fe_{73\%}V_{27\%}$ target. Hysteresis loops were measured under in-plane and perpendicular applied magnetic fields using a VSM for each sample with a given FeV thickness. The saturation magnetic moment per unit area ($M_s \times t_{\mathrm{FeV}}$) is then determined and used to obtain the magnetization at saturation (M_s) and the thickness of the magnetic dead layer (t_d) for each system. To investigate iDMI, BLS [14], under in-plane applied magnetic field in the Damon-Eshbach configuration was employed to record spectra for a given field and spin wave vector. For this, the sample is placed in the gap of an electromagnet generating an in-plane magnetic field up to 1.3 T. This sample is illuminated by a stabilized green laser (having a wavelength of $\lambda = 532$ nm) provided by an intense (200 mW) and monochromatic source with a long coherence length. The laser beam is then divided into two parts by a beam splitter: a reference beam used in the initial settings of the Fabry-Perrot tandem and the second part, used as a probe beam, is focused on the sample after passing through a set of several mirrors and lenses. The backscattered laser beam by the sample (elastic and inelastic processes) is oriented to a Fabry-Perot tandem to determine the frequency shift with a respect to the reference (Stokes and anti-Stokes) after passing through an analyzer to reduce the noise and eliminate the signal associated with the presence of the phonons. The wave vector (k_{sw}) is determined by the incidence angle of the laser (ϕ_{in}) through the relation: $k_{\mathrm{sw}} = \frac{4\pi}{\lambda}\sin(\phi_{\mathrm{in}})$. The Lorentzian fits of the BLS spectra were used to obtain the Stokes (S) and anti-Stokes (aS) line frequencies to investigate the variations of the frequency mismatch ($\Delta F = F_S - F_{aS}$) versus k_{SW} to measure the iDMI strength. Microstrip ferromagnetic resonance (MS-FMR) [15] was used to investigate PMA and damping. In these MS-FMR experiments, the samples, cut into pieces of 5×5 mm^2, are mounted on top of the signal line of a microstrip line which is connected to a microwave generator providing an excitation power of 20 dBm and to a Schottky detector used to measure the transmitted power. It is worth mentioning that a large excitation power drives magnetization precession in nonlinear region which complicates spectrum analysis and in particular the linewidth modelling. The magnetic field was swept (up to 1.6 T) at fixed frequency (up to 20 GHz) and once the FMR conditions are fulfilled, a strong absorption is clearly detected. The dimensions of the MS line are chosen to match the impedance of 50 Ω. To significantly increase the signal-to-noise ratio, a lock-in technique is employed. For this, two coils which sandwich the MS are inserted. These coils are driven by a power amplifier at 170 Hz, such that an alternating magnetic field of 0.4 mT can be produced to modulate the external applied magnetic field. The output signal of the Schottky detector is sent to the lock-in amplifier to obtain the experimental spectra which are proportional to the derivative of the absorbed power with respect to the applied field. These spectra are fitted with the Eq. (1) given in Ref. [16] to determine the resonance field (H_r) and the FMR field half linewidth at half maximum ΔH for a given driving frequency (F). For out-of-plane applied magnetic field measurements, the MS with the sample can be rotated around an in-plane axis from the in-plane direction ($\theta_H = \pm 90^\circ$, where θ_H is the angle defining the direction of the applied field and the normal to the film plane) to the normal to the layer plane ($\theta_H = 0$) by step of 5° while for in-plane applied field measurements, only the sample is rotated up to 360°. All the components of the MS-FMR setup are controlled by a computer via the Labview program operating under Windows, allowing adjusting, in real time, field steps, the excitation microwave frequency and the angle of the applied magnetic field as well as its intensity. The PMA and damping are investigate through the study of the frequency variation versus the magnetic field applied perpendicularly or in the plane of the film and via the frequency dependence of ΔH, respectively.

III. RESULTS AND DISCUSSIONS

Figure 1 shows the FeV thickness dependence of $M_s \times t_{\mathrm{FeV}}$, where the linear fits allow determining the magnetization at saturation (M_s) and the thickness of the magnetic dead layer (t_d): the slope gives M_s, while the horizontal axis intercept gives t_d. Similar values have been obtained for the Cu and MgO capped samples ($M_s = 1100 \pm 20$ kA/m and $t_d = 0.39 \pm 0.04$ nm). This magnetic dead layer could be due to the oxidation of the FeV during MgO layer deposition and interdiffusion at Ir/FeV and FeV/Cu interfaces. However, the similar t_d for both systems suggests the negligible oxidation or intermixing at FeV/MgO and Fe/Cu interfaces, confirming the immiscibility of Fe and Cu [17]. The M_s value is

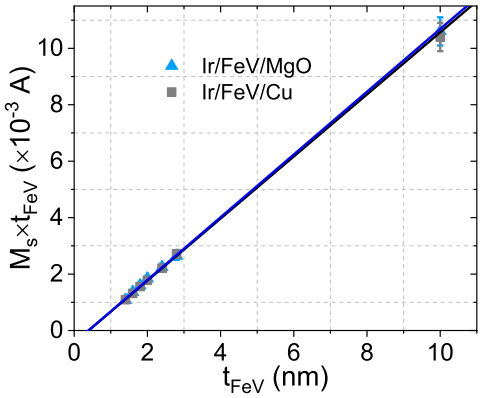

FIG. 1. Variation of the saturation magnetic moment per unit area versus the FeV thickness (t_{FeV}) for Ir/FeV/Cu and Ir/FeV/MgO systems. Symbols are VSM measurements data and lines refer to the linear fits.

significantly lower than that of pure Fe (1700 kA/m) [18] and bulk Co: 1422 kA/m for hcp Co and 1450 kA/m for fcc Co [19] reinforcing the interest of FeV for spin-transfer torque-based devices. The decrease of M_s with respect to that of Fe can be associated with the reduction of the Fe content and to the fact that V acquires a magnetic moment antiparallel to that the Fe atom moment [20]. For simplicity, all the measurements presented below are analyzed by considering $M_s = 1100$ kA/m and $t_d = 0.39$ nm to deduce PMA and iDMI parameters and investigate the thickness dependence of damping.

In order to estimate the stoichiometry of the FeV in our samples, we used available data on such systems in the literature. Devolder *et al.* [21] measured the V composition dependence of the magnetization at saturation of FeV of variable thicknesses (9–30 nm). The obtained values of M_s provided by Devolder *et al.* [21] revealed that M_s varies linearly with V content (x) as $\mu_0 M_s = (2.2-3x)$ [21] for $x < 0.4$. Using the measured value of M_s in our samples ($\mu_0 M_s = 1.382$ T), we estimated x to be 0.275, which is in good agreement with the nominal composition of the target.

We will now focus on the perpendicular magnetic anisotropy and Gilbert damping. For this aim, MS-FMR is first used to determine the gyromagnetic ratio ($\frac{\gamma}{2\pi} = g \times 13.97$ GHz/T, where g is the Landé factor) from the angular frequency ($\omega_\perp$) variation versus the amplitude of the perpendicular to the film plane applied magnetic field ($H_\perp$), as shown in Fig. 2(a) for Ir/FeV/MgO system with various t_{FeV}. Since $\omega_\perp = \mu_0 \gamma (H_\perp - M_{eff\perp})$, the linear fits of the data in Fig. 2(a) allow determining γ values and the perpendicular effective magnetization ($\mu_0 M_{eff\perp}$), from the slope and the horizontal axis intercept, respectively. The corresponding values of g, shown in the inset of Fig. 2(a), vary slightly with FeV thickness and therefore, for simplicity an average value of 2.13 will be used for both systems to analyse all measurements presented below.

After determining the gyromagnetic factor and $M_{eff\perp}$, measurements with an in-plane applied magnetic field were carried out to obtain the angular dependence of the resonance field and the field dependence of the uniform precession mode

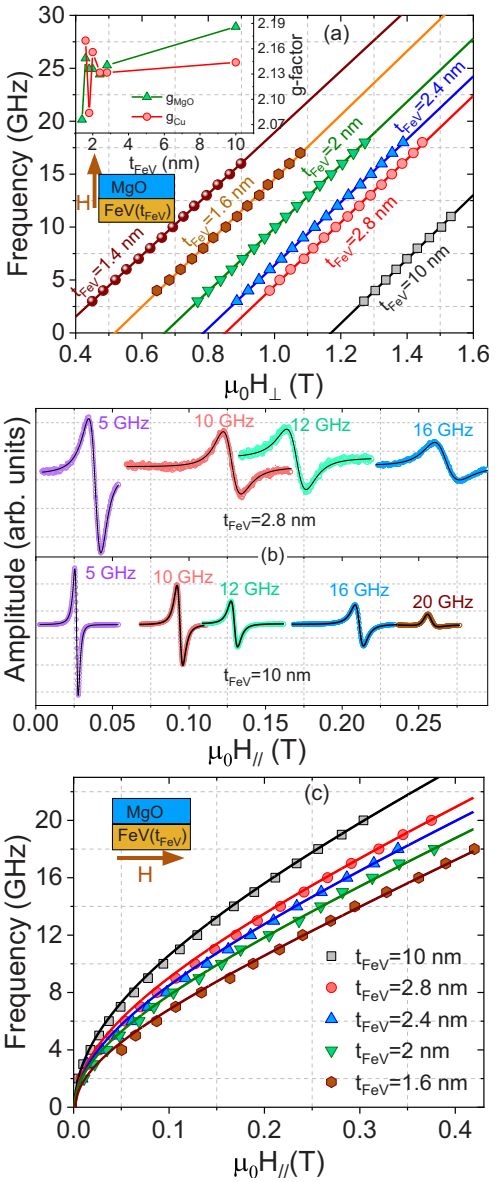

FIG. 2. Variations of the uniform precession mode frequency versus of (a) the perpendicular to the film plane ($H_\perp$) (c) the in-plane applied magnetic field ($H_\parallel$) for Pt/FeV(t_{FeV})/MgO system. Symbols refer to the experimental data and solid lines are fits using equations given in the paper. (b) MS-FMR spectra (measured at different microwave frequencies) representing the amplitude of the field derivative of the absorbed power as a function of the in-plane applied magnetic field for the 10-nm- and 2.8-nm-thick FeV films capped by MgO. The magnetic field was applied in the sample plane along the substrate edges. Symbols refer to experimental data and solid lines are fits using Eq. (1) of Ref. [16]. For more visibility, the amplitude of spectra at 5 GHz have been divided by 10 (6) for 10 nm (2.8 nm) FeV film.

frequency ($F_\parallel = \frac{\omega_{//}}{2\pi}$). The obtained typical MS-FMR spectra for different microwave frequencies and magnetic field applied along the substrate edges are shown in Fig. 2(b) for Ir/FeV/MgO system with 10- and 2.8-nm-thick FeV layers. Both the in-plane and the perpendicular to the film plane MS-FMR spectra (not shown here) were well defined, suggesting

a uniform composition and the absence of any significant segregated zones. The MS-FMR spectra recorded under in-plane and perpendicular to the film plane applied fields have been fitted with a derivative of a Lorentzian function given by Eq. (1) in Ref. [16] to determine ΔH and H_r for a given driving frequency (F) and a given direction. As illustrated by the spectra shown in Fig. 2(b), one should note the increase of ΔH and H_r as the thickness decreases due to the increase of PMA and damping as it will be commented below.

The in-plane angular variations of the resonance field revealed a weak uniaxial anisotropy that might be neglected, suggesting in-plane polycrystalline or amorphous structure of FeV grown on Si. This is expected in magnetron sputtered samples where the residual magnetic field of the magnetrons is expected to induce a weak uniaxial anisotropy even for amorphous or polycrystalline films. Therefore, the field dependences of the angular frequency $\omega_{\parallel}$, recorded for the applied field along the substrate edges and shown in Fig. 2(c), have been fitted with $\omega_{\parallel} = \mu_0\gamma\sqrt{H_{\parallel}(H_{\parallel} - M_{\text{eff}\parallel})}$ to deduce the in-plane effective magnetization ($M_{\text{eff}\parallel}$).

The obtained values of $\mu_0 M_{\text{eff}\parallel}$ and $\mu_0 M_{\text{eff}\perp}$ for Ir/FeV/MgO and Ir/FeV/Cu are shown in Fig. 3(a) versus the inverse of the FeV effective thickness defined as $t_{\text{eff}} = t_{\text{FeV}} - t_d$. Interestingly, one can observe a significant difference between $\mu_0 M_{\text{eff}\parallel}$ and $\mu_0 M_{\text{eff}\perp}$ in both systems suggesting the existence of a second-order PMA constant $K_{2\perp}$ besides the uniaxial PMA constant $K_{\perp}$. Note that sometimes in literature, these anisotropy constants are also referred to as second-order and fourfold anisotropy constants. Indeed, according to the model in Ref. [16], the out-of-plane angular dependence of the precession frequency is given by Eq. (1), where $\theta_M(\theta_H)$ refers to the out-of-plane angle defining the direction of the magnetization (the applied field) and the normal to the film plane. Therefore, for in-plane applied magnetic fields, the contribution of $K_{2\perp}$ to the frequency vanishes and $\mu_0 M_{\text{eff}\parallel} = \mu_0 M_s - \frac{2K_{\perp}}{M_s}$. However, for a perpendicular applied magnetic field, the frequency is $K_{2\perp}$ dependent and the extracted $M_{\text{eff}\perp}$ is defined as $\mu_0 M_{\text{eff}\perp} = \mu_0 M_s - \frac{2K_{\perp}}{M_s} - \frac{4K_{2\perp}}{M_s}$. Therefore, $K_{2\perp}$ can be deduced from the difference between $\mu_0\, M_{\text{eff}\parallel}$ and $\mu_0\, M_{\text{eff}\perp}$ as shown in the inset of Fig. 3(a) for both systems.

$$\omega_{\text{Out}} = \mu_0\gamma\sqrt{\frac{\left[H\cos(\theta_M - \theta_H) - M_{\text{eff}\parallel}\cos(2\theta_M) + \frac{2K_{2\perp}}{\mu_0 M_S}(\cos(2\theta_M) + \cos(4\theta_M))\right]}{\left[H\cos(\theta_M - \theta_H) - M_{\text{eff}\parallel}\cos^2(\theta_M) + \frac{4K_{2\perp}}{\mu_0 M_S}\cos^4(\theta_M)\right]}}. \quad (1)$$

Note the negative sign of the $K_{2\perp}$ reinforcing the in-plane easy axis of the magnetization. The extent of $K_{2\perp}$ variations versus $1/t_{\text{eff}}$ of Cu capped samples is approximately twice that of Ir/FeV/MgO system. Furthermore, $K_{2\perp}$ increases in absolute value with the decreasing FeV thickness and rather saturates for $t_{\text{FeV}} = 2$ nm in Ir/FeV/Cu. We should mention that the out-of-plane angular dependence of the resonance field [shown in Fig. 3(b)] could not be fitted by Eq. (1) without the use of $K_{2\perp}$. It is worth mentioning that inhomogeneous distribution and spatial fluctuations at the nanoscale of the uniaxial anisotropy at interfaces could be responsible for the presence of $K_{2\perp}$ [22,23].

Let us now come back to the thickness dependence of effective magnetization where the linear dependence suggests the existence of an interfacial contribution to the PMA. This interfacial contribution to PMA is of utmost importance to spintronic applications, since it offers the possibility to tune the effective anisotropy field via thickness to a desired value. The deviation from the linear behavior for the thinner FeV films is most likely due to interface quality degradation as the thickness is reduced. This deviation is more pronounced for Cu capped samples most probably due to the increased structural disorder, interfacial inhomogeneity and roughness, in line with the higher values of $K_{2\perp}$ compared to the MgO capped films. Furthermore, this deviation from the linearity is more obvious in the variations of $\mu_0 M_{\text{eff}\perp}$ versus $1/t_{\text{eff}}$, since $\mu_0 M_{\text{eff}\perp}$ is affected by $K_{2\perp}$, in contrast to $\mu_0 M_{\text{eff}\parallel}$. Due to the linear dependence of $\mu_0 M_{\text{eff}\parallel}$ versus $1/t_{\text{eff}}$, $K_{\perp}$ can be described by the phenomenological relationship $K_{\perp} = K_v + \frac{K_s}{t_{\text{eff}}}$, where K_{s} and K_{v} are the perpendicular uniaxial surface and volume anisotropy constants, respectively. K_{v} and K_{s} are directly obtained from the intercept and from the slope of the linear fit of $\mu_0 M_{\text{eff}\parallel}$ versus $1/t_{\text{eff}}$, as shown in Fig. 3(a). The obtained values are summarized in Table I, where both systems show almost similar values of K_{s} and K_{v}. Despite the similar obtained values of K_s for both systems, it is difficult to precisely determine the interface inducing such PMA since FeV/Cu and FeV/MgO could contribute to K_{s} besides Ir/FeV interface. However, one could expect that the contribution of the top interface with FeV, in both systems, to be negligible, especially that of FeV/MgO where Fe–O bonds, which are a source of the interfacial PMA, are expected to occur. This suggests that V could reduce significantly Fe–O bonds at the FeV/MgO interface and thus preventing any contribution to PMA. This could be elucidated by investigating Cu/FeV/Cu systems.

The FMR linewidth gives information about the magnetization relaxation and samples inhomogeneities. The frequency dependences of ΔH are shown in Figs. 4(a) and 4(b) for Ir/FeV/MgO samples. Note the significantly lower ΔH for a perpendicular to the plane applied magnetic field most probably due to the two magnon scattering contribution to ΔH when the magnetic field is applied in the film plane [Fig. 4(b)]. The two magnon scattering contribution, which is related to scatterings on local inhomogeneities or interfaces, is confirmed by the out-of-plane angular dependence of ΔH, as shown in Figs. 4(c) and 4(d) for two MgO-capped samples with 2.8-nm- and 10-nm-thick FeV films. Indeed, as we move from in-plane to out-of-plane, ΔH increases drastically before decreasing significantly in the vicinity of the normal direction and reaching its minimum, as predicted by the two magnon scattering model [24]. The angular dependences of ΔH shown in Figs. 4(c) and 4(d) were fitted by considering the contributions of two magnon scattering

TABLE I. Parameters obtained from the best fits of the effective magnetization, the damping and the effective iDMI constant versus the inverse of the effective thickness of FeV thin films grown on Si substrates using MgO or Cu capping layers.

System	M_s (kA/m)	K_v ($\times 10^5$ J/m^3)	K_s (mJ/m^2)	$\alpha_{\mathrm{FeV}\parallel}$ ($\times 10^{-3}$)	$\alpha_{\mathrm{FeV}\perp}$ ($\times 10^{-3}$)	$g^{\uparrow\downarrow}_{\mathrm{eff}\parallel}$ (nm^{-2})	$g^{\uparrow\downarrow}_{\mathrm{eff}\perp}$ (nm^{-2})	D_s (pJ/m)
Ir/FeV/MgO	1112 ± 20	0.77 ± 0.08	0.57 ± 0.04	2.77 ± 0.72	1.75 ± 0.67	26.18 ± 2.9	22.22 ± 1.9	0.06 ± 0.01
Ir/FeV/Cu	1100 ± 16	0.65 ± 0.09	0.63 ± 0.08	3.78 ± 0.55	1.67 ± 0.92	27.71 ± 2.2	24.52 ± 2.5	0.13 ± 0.02

and mosaicity besides that of Gilbert and inhomogeneities. For the sake of simplicity, because additional theoretical considerations would be required to fit ΔH versus the out-of-plane direction of the applied magnetic field, we limited our investigation of damping to the measurements with perpendicular applied magnetic fields where the two magnon scattering contribution vanishes. For comparison and to evaluate the contribution of the two magnon scattering, damping values with an in-plane magnetic field have also been considered. Furthermore, a pronounced two magnon scattering contribution to ΔH results in nonlinearity of the frequency dependence of ΔH for an in-plane applied magnetic field. The absence of such pronounced nonlinearity in the frequency dependence of the in-plane ΔH [see Figs. 4(a) and 4(b)] makes difficult the separation of the Gilbert-type damping contribution and the two magnon scattering contribution to ΔH.

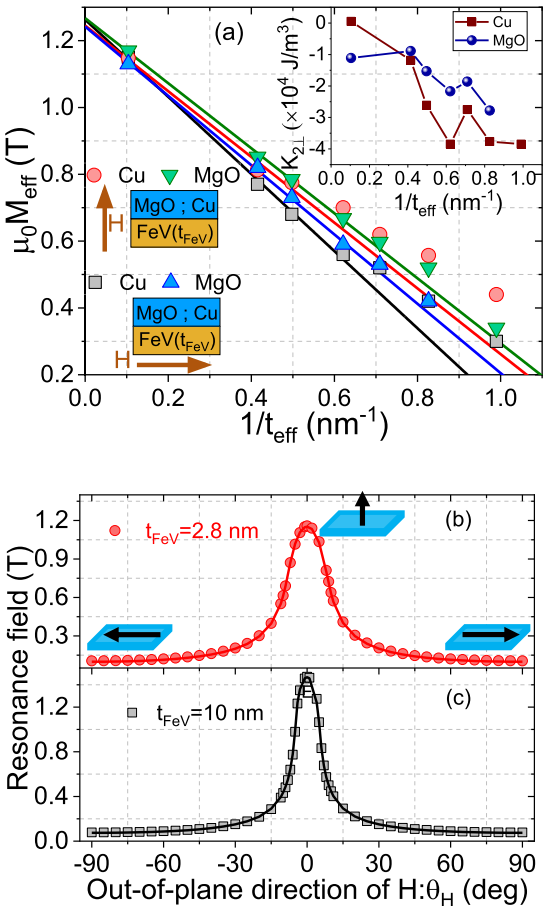

FIG. 3. (a) Eeffective magnetization ($\mu_0 M_{\mathrm{eff}}$) versus the FeV reciprocal effective thickness ($1/(t_{\mathrm{FeV}} - t_d)$) of Pt/FeV($t_{\mathrm{FeV}}$)/MgO and Pt/FeV($t_{\mathrm{FeV}}$)/Cu systems grown on Si substrates. $\mu_0 M_{\mathrm{eff}}$ values have been extracted from the fit of MS-FMR measurements of the frequency of the uniform precession mode versus the in-plane and the perpendicular applied magnetic field using equations given in the main text. Symbols refer to experimental data while solid lines are the linear fits taking into account only the thicker films. The inset shows the second- order perpendicular magnetic anisotropy constant versus the FeV reciprocal effective thickness of the corresponding systems. Solid lines are used as guides to the eye. Variation of the resonance field versus of the out-of-plane angle measured at 9 GHz driving frequency for Ir/FeV/MgO system with (b) 2.8-nm- and (c) 10-nm-thick FeV layer. θ_H refers to the out-of-plane angle defining the direction of the applied field and the normal to the film plane. Symbols refer to experimental data and solid lines are fits using Eq. (1).

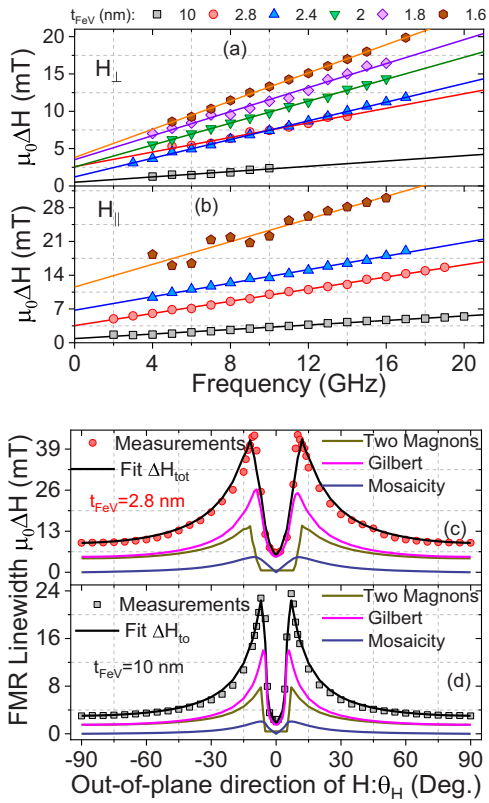

FIG. 4. FMR half width at half maximum linewidth (ΔH) versus the driving frequency for (a) in-plane or (b) perpendicular to the film plane applied magnetic field of Ir/FeV(t_{FeV})/MgO of various FeV thicknesses. Symbols refer to experimental data and solid lines are linear fits. Variation of ΔH versus the direction of the out-of-plane applied magnetic field with a respect to the normal to the sample plane (θ_H) measured at 9 GHz driving frequency for Ir/FeV/MgO system with (c) 2.8-nm- and (d) 10-nm-thick FeV layer. Symbols refer to experimental data and solid lines are fits using Gilbert, two magnon and mosaicity contribution.

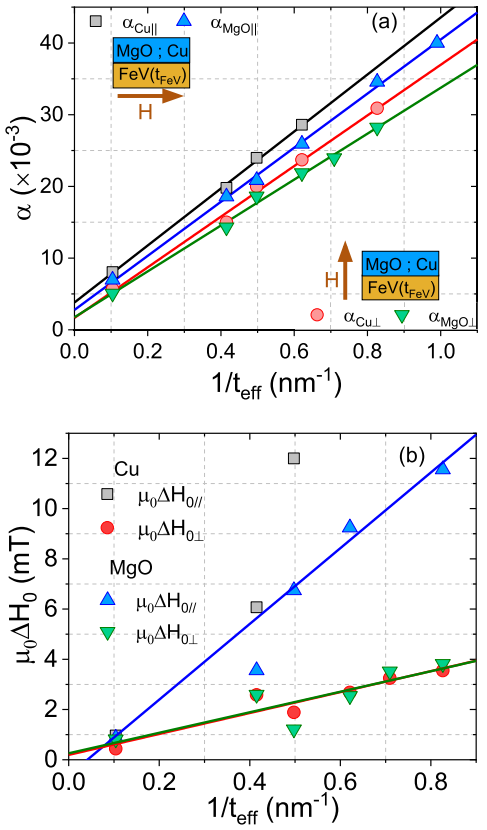

FIG. 5. (a) Gilbert damping parameter and (b) zero frequency linewidth, deduced from in-plane ($\parallel$) and perpendicular ($\perp$) applied magnetic fields measurements, as a function of the FeV reciprocal effective thickness of Ir/FeV(t_{FeV})/MgO and Ir/FeV(t_{FeV})/Cu systems. Symbols refer to experimental data and solid lines are linear fits.

Therefore, the frequency dependences of ΔH have been fitted by $\mu_0\Delta H = \mu_0\Delta H_0 + \frac{2\pi}{\gamma}\alpha F = \mu_0\Delta H_0 + \frac{\omega}{\gamma}\alpha$ to determine the magnetic damping (α) and the inhomogeneous contribution (ΔH_0) for both systems and for each configuration of the applied field. This leads to the real Gilbert damping ($\alpha_\perp$) or to an effective damping constant ($\alpha_\parallel$), including the two magnon contribution when fitting the perpendicular or the in-plane ΔH, respectively. The variations of α as a function of $1/t_{\text{eff}}$ are shown Fig. 5(a) for both systems and for both in-plane and perpendicular to the plane applied magnetic fields. Note the linear dependence of α versus $1/t_{\text{eff}}$ with a slight variation of the slope with the capping layer: the slope is lower for MgO capped samples, suggesting that the damping increase is mainly induced by the spin pumping at the Ir/FeV. It also supports the assertion that MgO does not permit a spin current to flow to Ta and suppresses spin pumping at the top interface with FeV, in contrast to Cu capped samples [25]. We thus consider that the total damping is given by $\alpha = \alpha_{\text{FeV}} + \alpha_P$, where α_{FeV} is the Gilbert damping constant of the FeV. $\alpha_P = \frac{g\mu_B}{4\pi M_s t_{\text{eff}}} g_{\text{eff}}^{\uparrow\downarrow}$ (where μ_B is the Bohr magneton and $g_{\text{eff}}^{\uparrow\downarrow}$ is the effective spin mixing conductance) is the damping induced by the spin pumping effect. The linear fits of the experimental data give α_{FeV} and $g_{\text{eff}}^{\uparrow\downarrow}$ from the vertical axis intercept and the slope, respectively. The results for both systems and field configurations are shown in Table I. The obtained values confirm the low Gilbert damping constant of FeV ($\alpha_{\text{FeV}} = 1.7 \times 10^{-3}$), which is in good agreement with the reported value by Arora *et al.* [26]. It also allowed concluding that damping enhancement is mainly induced by Ir/FeV while the contribution of the top interface is significantly lower. Note the higher values of α_{FeV} and $g_{\text{eff}}^{\uparrow\downarrow}$ deduced from the linear fit of $\alpha_\parallel$ versus $1/t_{\text{eff}}$ resulting from the two magnon scattering. However, while its contribution to α_{FeV} is significant leading to overestimation of α_{FeV} which can be up to a factor 2, its contribution to $g_{\text{eff}}^{\uparrow\downarrow}$ is weak, suggesting a negligible interfacial two magnon scattering. It is worth noticing the slight higher values of α_{FeV} and $g_{\text{eff}}^{\uparrow\downarrow}$ of the Cu capped samples compared to those of Ir/FeV/MgO due the suppression of spin pumping by MgO at the top interface and the relatively stronger two magnon scattering in Ir/FeV/Cu which could be partially due to more structural disorder and roughness at the interfaces with Cu.

ΔH_0 is associated with an extrinsic contribution to the linewidth and reflects the magnetic and structural inhomogeneities in the layers and two magnon scatterings due to defects. In-plane and perpendicular FMR measurements of ΔH allow one to separate inhomogeneity and two magnon scattering contributions, since for inhomogeneities, a line broadening in the perpendicular configuration is expected compared to the parallel configuration. Therefore, the thickness dependence of the $\Delta H_{0\parallel}$ and $\Delta H_{0\perp}$, deduced from the linear fit of the frequency dependence of ΔH under in-plane or perpendicular applied magnetic field, was investigated as shown in Fig. 5(b). For both systems, $\Delta H_{0\parallel}$ is significantly higher than $\Delta H_{0\perp}$, especially for the thinner FeV films suggesting that $\Delta H_{0\parallel}$ results mainly from two magnon scattering contributions. Indeed, $\Delta H_{0\parallel} \approx \Delta H_{0\perp}$ for thicker FeV ($t_{\text{FeV}} = 10$ nm) and as t_{FeV} decreases ΔH_0 increases and the gap between $\Delta H_{0\parallel}$ and $\Delta H_{0\perp}$ becomes more significant. The substantially higher values of $\Delta H_{0\parallel}$ of Cu capped FeV films is most probably due to more imperfections and inhomogeneities. However, the lack of sufficient data for these samples with thinner FeV films due to the weak FMR signal under in-plane applied magnetic field does not allow us to conclude on the origin of $\Delta H_{0\parallel}$ and its thickness dependence in such samples. In contrast, the linear dependence of ΔH_0 versus $1/t_{\text{eff}}$ reflects the interfacial nature of imperfections and inhomogeneities at the origin of ΔH_0 in MgO capped samples.

We have also investigated iDMI in both systems, which can be determined through the investigation of the frequency mismatch ΔF between spin wave frequencies corresponding to Stokes and anti-Stokes lines. Due to the weak iDMI values that could be induced by Ir/FM interface, we limited the determination of the iDMI effective constant (D_{eff}) to frequency mismatch ΔF measurements at maximal $k_{\text{sw}} = 20.45\ \mu\text{m}^{-1}$ (corresponding to $\phi_{\text{in}} = 60°$) without crossed analyzer. This allows probing bulk phonon and magnon Stokes and anti-Stokes lines. The acoustic waves are used to check the zero frequency setting and proceed to frequency correction (in case of incorrect adjustment of the zero frequency) for a precise measurement of the iDMI constant [27]. D_{eff} is determined from the relation $\Delta\omega = 2\pi\,\Delta F = D_{\text{eff}}\frac{4\gamma}{M_s}k_{\text{sw}} =$

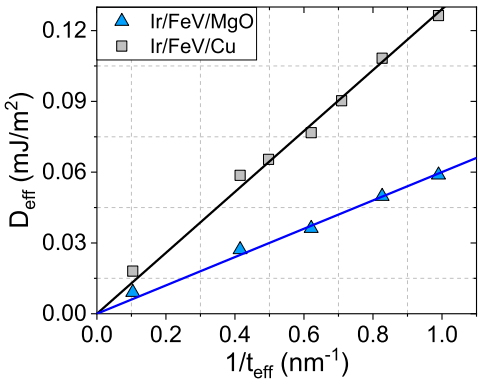

FIG. 6. Variation of the effective iDMI constants as a function of the FeV reciprocal effective thickness of Ir/FeV(t_{FeV})/MgO and Ir/FeV(t_{FeV})/Cu systems. Solid lines refer to the linear fit and symbols are experimental data.

$D_s \frac{4\gamma}{M_s t_{\mathrm{eff}}} k_{\mathrm{sw}}$, where $D_{\mathrm{eff}} = D_s/t_{\mathrm{eff}}$ and D_s is the iDMI surface constant, characterizing the iDMI strength and $k_{\mathrm{sw}} = 20.45\ \mu\mathrm{m}^{-1}$. The variation of D_{eff} versus $1/t_{\mathrm{eff}}$ for both systems, shown in Fig. 6, reveals a linear behavior allowing us to determine D_s for each system as shown in Table I. Apart from the $1/t_{\mathrm{eff}}$ dependence and the weak iDMI, one can observe a significant difference between Cu and MgO capped samples, suggesting a contribution from the top interface. In order to deepen the analysis and to have an estimation of the iDMI strength of each interface, we consider that both FeV interfaces are sufficiently apart so that they give distinct contributions to the iDMI [28]. Therefore, the total iDMI constant is $D_s^{\mathrm{Ir/FeV/MgO}} = D_s^{\mathrm{Ir/FeV}} + D_s^{\mathrm{FeV/MgO}}$ and $D_s^{\mathrm{Ir/FeV/Cu}} = D_s^{\mathrm{Ir/FeV}} + D_s^{\mathrm{FeV/Cu}}$ for Ir/FeV/MgO and Ir/FeV/Cu, respectively. Since for both systems, the growth process is similar up to the FeV layer, we can assume that the iDMI strength at the Ir/FeV interface does not change from one system to another. Considering that $D_s^{\mathrm{FeV/Cu}} = 0$, we deduce $D_s^{\mathrm{Ir/FeV}} = (0.13 \pm 0.02)$ pJ/m and $D_s^{\mathrm{FeV/MgO}} = (-0.07 \pm 0.02)$ pJ/m. This latter value is lower than the deduced value of Fe/MgO ($D_s^{\mathrm{Fe/MgO}} = -0.15$ pJ/m) [29], Co/MgO ($D_s^{\mathrm{Co/MgO}} = -0.22$ pJ/m) [30], and CoFeB/MgO ($D_s^{\mathrm{CoFeB/MgO}} = -0.17$ pJ/m) [30] from measurements reported in Refs. [29,30]. The obtained value of $D_s^{\mathrm{Ir/FeV}}$ is also significantly lower than that of Co/Ir ($D_s^{\mathrm{Co/Ir}} = 0.32$ pJ/m) [31] and could be attributed to different details of the interface morphology since iDMI is sensitive to the atomic arrangements at the interface. Note the positive sign of iDMI constant of Ir/FeV similar to that of Ir/Fe and opposite to that of Ir/Co. Moreover, $D_s^{\mathrm{Ir/FeV}}$ is significantly lower than the reported iDMI energy value of ∼4 meV/atom thus $D_{\mathrm{eff}} \sim 7\ \mathrm{mJ/m^2}$ ($D_s \sim 2.1$ pJ/m) at 11 K by scanning tunnel microscope measurements [32] for Ir/Fe interface. We should mention that the investigation of Heinze *et al.* [32] concerns a low temperature measurements on a Fe ML grown pseudomorphically on a hexagonal Ir(111) surface, which is a perfect ultrathin layer. In the absence of the temperature dependence of D_s, it is difficult to predict its value at room temperature and thus to compare with the obtained value for FeV. However, Zhang *et al.* [29] reported iDMI measurements at room temperature on Ir/Fe(3nm)/SiO_2, where $D_{\mathrm{eff}} \sim 0.3\ \mathrm{mJ/m^2}$ ($D_s \sim 0.6$ pJ/m) are obtained. While the iDMI sign of Ir/Fe is in good agreement with that of Ir/FeV, the strength of the iDMI induced by the latter is weaker. Moreover, in our previous work [31], we showed that the Ir/Co and Co/Ir interfaces present different iDMI: while D_s of Co/Ir is 0.29 pJ/m no iDMI is induced by the Ir/Co interface. It is not surprising to obtain such weak iDMI induced bat Ir/FeV. We should mention that iDMI is sensitive to disorder, defects, and atom arrangement at the interfaces which vary significantly as a function of sample elaboration parameters, like deposition technique, underlayer, and capping layer. Therefore, it is not surprising to have dispersion between experiments for the obtained values of iDMI since the sample elaboration and interface properties may differ.

Stabilization of skyrmions results from the competition between iDMI, symmetric exchange and the effective perpendicular anisotropy. Therefore, it is important to compare the exchange stiffness constant (A_{ex}) of FeV to the iDMI constant. Since the primary goal of the investigation is the interfacial phenomena, ultrathin films are needed (<10 nm). For such thinner films, the perpendicular standing spin wave frequencies, needed to estimate A_{ex}, overpass the frequency range available in our FMR setup. Even with BLS, due to the lower signal-to-noise ratio, it is difficult to determine precisely A_{ex} of such ultrathin FeV films. However, according to Devolder *et al.* [21], A_{ex} of FeV is in the range of 22–26 pJ/m for x below 0.4 and is essentially independent of the vanadium content. Therefore, D_s of Ir/FeV is very weak compared to A_{ex}. We should mention that in all the studied systems in literature, A_{ex} is always significantly higher than the iDMI constant even for the Pt/Co/MgO system where the higher iDMI values are measured ($D_s = -2.17$ pJ/m [33]). This is not surprising since A_{ex} characterizes the symmetric direct exchange interaction between spins and D_s refers to the strength of the indirect antisymmetric exchange interaction between spins through a heavy metal atom. The symmetric exchange interaction is thus of longer range (defined by the exchange length) compared to iDMI which is more localized at interface. Furthermore, in contrast to A_{ex} which depends on the ferromagnetic materials, the D_s values depend mainly on the heavy metal nature.

Let us now discuss the applicative potential of FeV. The composition dependence of the damping parameters of Fe, Co, Ni, and their alloys has been reported by Oogane *et al.* [34]. The bulk Fe has the lower damping ($\alpha = 1.9 \times 10^{-3}$) when compared to Co ($\alpha = 11 \times 10^{-3}$) and Ni ($\alpha = 64 \times 10^{-3}$). FeCo alloys with a high Fe content show minimal values ($Co_{25}Fe_{75}$) then the damping parameter gradually increased with the increasing Co. For NiCo alloys, the damping parameter remains in the range $11 \times 10^{-3} \leqslant \alpha \leqslant 19 \times 10^{-3}$ with Ni concentration between 10 and 70%. Compared to Fe, Co, and Ni, FeV is a particularly attractive material for spintronic applications due to its lower damping constant ($\alpha \sim 1.7 \times 10^{-3}$). It is worth mentioning that the dispersion of α values of these ferromagnetic materials is noted in the literature [35]. Despite its α comparable to that of bulk Fe, its M_s is significantly lower making it possible to achieve spontaneously perpendicular magnetized films with a reasonable thickness, needed for wide variety of spintronic devices. In

summary, FeV has a low damping constant ($\alpha \sim 1.7 \times 10^{-3}$), a moderate M_s and a low effective anisotropy field (for ultrathin films) which allow for efficient reversal of magnetization through dampinglike SOT due to the SHE. We should mention that these three parameters could be further tuned by a judicious choice of V content, FeV thickness, capping, and buffer layers. The choice of FeV as a material for spintronic application is thus particularly advantageous as it combines the low damping and the reduced magnetization compared to Fe as well as interface anisotropy to achieve PMA materials. Therefore, FeV could be particularly attractive material for spintronic applications.

IV. CONCLUSION

Magnetic damping, interfacial Dzyaloshinskii-Moriya interaction and perpendicular magnetic anisotropy, which are technological key parameters, were investigated in Ir/FeV/Cu and Ir/FeV/MgO by ferromagnetic resonance and Brillouin light scattering. The analysis of the experimental data reveals the existence of a uniaxial perpendicular magnetic interface anisotropy which shows slight capping layer dependence suggesting that it is mainly induced by Ir/FeV interface. In contrast, the second-order PMA constant which could arise from the inhomogeneous distribution and the spatial fluctuations at the nanoscale of the uniaxial PMA at interface, is significantly stronger for the Ir/FeV/Cu system. FMR measurements of the linewidth under in-plane and perpendicular applied magnetic field allowed us to conclude on a relatively low Gilbert damping constant of FeV ($\alpha_{\mathrm{FeV}} = 1.7 \times 10^{-3}$) and to identify inhomogeneities and two magnon scattering contributions. While the zero frequency linewidth in the plane results mainly from two magnon scattering for both systems, ΔH_0 in the perpendicular configuration is due to interfacial inhomogeneities. Damping enhancement was observed and attributed to spin pumping at the Ir/FeV interface. The thickness dependence of the effective iDMI constant was investigated and allowed to separate the contributions of the various interfaces. Our results show that Ir/FeV and FeV/MgO interfaces induce a weak iDMI of opposite sign leading to additional contribution to the total iDMI.

ACKNOWLEDGMENTS

We acknowledge the French National Research Agency for financial support within the ANR program EHIS (ANR-21-CE42-0003). M.S.G. acknowledges the financial support for this work from MRID, CNCS/CCCDI—UEFISCDI, through Grant PN-III-P4-ID-PCE-2020-1853-SPINSYNE.

[1] J. Ding, C. Liu, Y. Zhang, U. Erugu, Z. Quan, R. Yu, E. McCollum, S. Mo, S. Yang, H. Ding, X. Xu, J. Tang, X. Yang, and M. Wu, Phys. Rev. Appl. **14**, 014017 (2020).

[2] V. V. Kruglyak, S. O. Demokritov, and D. Grundler, J. Phys. D **43**, 264001 (2010).

[3] R. M. Rowan-Robinson, A. T. Hindmarch, and D. Atkinson, J. Appl. Phys. **124**, 183901 (2018).

[4] K. Gilmore, Y. U. Idzerda, and M. D. Stiles, Phys. Rev. Lett. **99**, 027204 (2007).

[5] I. Turek, J. Kudrnovský, and V. Drchal, Phys. Rev. B **92**, 214407 (2015).

[6] B. Khodadadi, A. Rai, A. Sapkota, A. Srivastava, B. Nepal,Y. Lim, D. A. Smith, C. Mewes, S. Budhathoki, A. J. Hauser, M. Gao, J.-F. Li, D. D. Viehland, Z. Jiang, J. J. Heremans, P. V. Balachandran, T. Mewes, and S. Emori, Phys. Rev. Lett. **124**, 157201 (2020).

[7] V. Kambersky and C. E. Patton, Phys. Rev. B **11**, 2668 (1975).

[8] S. Mizukami, D. Watanabe, M. Oogane, Y. Ando, Y. Miura, M. Shirai, and T. Miyazaki, J Appl. Phys. **105**, 07D306 (2009).

[9] P. Dürrenfeld, F. Gerhard, J. Chico, R. K. Dumas, M. Ranjbar, A. Bergman, L. Bergqvist, A. Delin, C. Gould, L. W. Molenkamp, and J. Åkerman, Phys. Rev. B **92**, 214424 (2015).

[10] C. Scheck, L. Cheng, I. Barsukov, Z. Frait, and W. E. Bailey, Phys. Rev. Lett. **98**, 117601 (2007).

[11] J. Sinova, S. O. Valenzuela, J. Wunderlich, C. H. Back, and T. Jungwirth, Rev. Mod. Phys. **87**, 1213 (2015).

[12] A. Crépieux and C. Lacroix, J. Magn. Magn. Mater. **182**, 341 (1998).

[13] H. Yang, S. Hu, M. Tang, S. Chen, H. Chen, D. Wu, and X. Qiu, Appl. Phys. Lett. **118**, 062409 (2021).

[14] M. Belmeguenai, M. S. Gabor, Y. Roussigné, A. Stashkevich, S. M. Chérif, F. Zighem, and C. Tiusan, Phys. Rev. B **93**, 174407 (2016).

[15] M. Belmeguenai, M. S. Gabor, F. Zighem, N. Challab, T. Petrisor, Jr., R. B. Mos, and C. Tiusan, J. Phys. D **51**, 045002 (2018).

[16] I. Benguettat-EL Mokhtari, Y. Roussigné, T. Petrisor, Jr., F. Zighem, F. Kail, L. Chahed, V. Pierron, L. Méchin, M. Gabor, and M. Belmeguenai, Phys. Status Solidi B **257**, 2000265 (2020).

[17] M. Sun, A. Rauf, Y. Zhang, G. Sha, G. Peng, Z. Yu, C. Guo, Y. Fang, S. Lan, T. Feng, H. Hahn, and H. Gleiter, Mater. Res. Lett. **6**, 55 (2018).

[18] J.-M. L. Beaujour, A. D. Kent, D. W. Abraham, and J. Z. Sun, J. Appl. Phys. **103**, 07B519 (2008).

[19] Y. C. Won and S. H. Lim, Sci. Rep. **11**, 10779 (2021).

[20] I. Mirebeau, G. Parette, and J. W. Cable, J. Phys. F **17**, 191 (1987).

[21] T. Devolder, T. Tahmasebi, S. Eimer, T. Hauet, and S. Andrieu, Appl. Phys. Lett. **103**, 242410 (2013).

[22] A. A. Timopheev, R. Sousa, M. Chshiev, H. T. Nguyen, and B. Dieny, Sci. Rep. **6**, 26877 (2016).

[23] J. B. Mohammadi, K. Cole, T. Mewes, and C. K. A. Mewes, Phys. Rev. B **97**, 014434 (2018).

[24] R. D. McMichael, D. J. Twisselmann, and A. Kunz, Phys. Rev. Lett. **90**, 227601 (2003).

[25] A. A. Baker, A. I. Figueroa, D. Pingstone, V. K. Lazarov, G. van der Laan, and T. Hesjedal, Sci. Rep. **6**, 35582 (2016).

[26] M. Arora, E. K. Delczeg-Czirjak, G. Riley, T. J. Silva, H. T. Nembach, O. Eriksson, and J. M. Shaw, Phys. Rev. Appl. **15**, 054031 (2021).

[27] D. Ourdani, Y. Roussigné, S. M. Chérif, M. S. Gabor, and M. Belmeguenai, J. Phys. D **55**, 485004 (2022).

[28] F. Ajejas, V. Krizakova, D. de Souza Chaves, J. Vogel, P. Perna, R. Guerrero, A. Gudin, J. Camarero, and S. Pizzini, Appl. Phys. Lett. **111**, 202402 (2017).

[29] W. Zhang, B. Jiang, L. Wang, Y. Fan, Y. Zhang, S. Y. Yu, G. B. Han, G. L. Liu, C. Feng, G. H. Yu, S. S. Yan, and S. Kang, Phys. Rev. Appl. **12**, 064031 (2019).

[30] X. Ma, G. Yu, C. Tang, X. Li, C. He, J. Shi, Kang L. Wang, and Xiaoqin Li, Phys. Rev. Lett. **120**, 157204 (2018).

[31] I. Benguettat-El Mokhtari, D. Ourdani, Y. Roussigné, R. B. Mos, . M. Nasui, F. Kail, L. Chahed, S. M. Chérif, A. Stashkevich, M. Gabor, and M. Belmeguenai, J. Phys.: Condens. Matter **32**, 495802 (2020).

[32] S. Heinze, K. von Bergmann, M. Menzel, J. Brede, A. Kubetzka, R. Wiesendanger, G. Bihlmayer, and S. Blügel, Nat. Phys. **7**, 713 (2011).

[33] O. Boulle, J. Vogel, H. Yang, S. Pizzini, D. de Souza Chaves, A. Locatelli, T. O. Menteş, A. Sala, L. D. Buda-Prejbeanu, O. Klein, M. Belmeguenai, Y. Roussigné, A. Stashkevich, S. M. Chérif, L. Aballe, M. Foerster, M. Chshiev, S. Auffret, I. M. Miron, and G. Gaudin, Nat. Nanotechnol. **11**, 449 (2016).

[34] M. Oogane, T. Wakitani, S. Yakata, R. Yilgin, Y. Ando, A. Sakuma, and T. Miyazai, Jpn. J. Appl. Phys. **45**, 3889 (2006).

[35] S. J. Xu, J. Y. Shi, Y. S. Hou, Z. Zheng, H. B. Zhao, R. Q. Wu, S. M. Zhou, Z. Shi, and W. J. Fan, Phys. Rev. B **100**, 024403 (2019).